A Simplified Method for Preparation of ^{99m}Tc-Annexin V and its Biologic Evaluation for In Vivo Imaging of Apoptosis After Photodynamic Therapy

Murugesan Subbarayan, PhD[1]; Urs O. Häfeli, PhD[2]; Denise K. Feyes, MS[3]; Jaya Unnithan, MD[2]; Steven N. Emancipator, MD, PhD[4]; and Hasan Mukhtar, PhD[1]

[1]Department of Dermatology, University of Wisconsin, Madison, Wisconsin; [2]Department of Radiation Oncology, The Cleveland Clinic Foundation, Cleveland, Ohio; [3]Department of Dermatology, Case Western Reserve University, Cleveland, Ohio; and [4]Department of Pathology, Case Western Reserve University, Cleveland, Ohio

Apoptosis is the likely mechanism behind the effects of chemotherapeutic and radiation treatments, rejection of organ transplants, and cell death due to hypoxic-ischemic injury. A simplified method capable of imaging apoptosis in living animals could have many applications leading to understanding of the involvement of apoptosis in biologic and therapeutic processes. To accomplish this goal we developed a method for the preparation of ^{99m}Tc-annexin V and evaluated its usefulness to detect apoptosis that occurs during tumor shrinkage after photodynamic therapy (PDT). PDT is a cancer treatment modality that leads to rapid induction of apoptosis both in vitro and in in vivo animal models. **Methods:** A novel synthesis of ^{99m}Tc-annexin V was performed in a simple 1-pot procedure. Radiation-induced fibrosarcoma (RIF-1) tumors grown in C_3H mice were treated with PDT, followed by injection of ^{99m}Tc-annexin V and measurement of its tumor uptake at 2, 4, and 7 h after PDT by autoradiography. **Results:** The radiochemical purity of ^{99m}Tc-annexin V was >95%. At all time points, ^{99m}Tc-annexin V was clearly imaged in the PDT-treated tumors, whereas the untreated tumors showed no uptake of the radiolabeled compound. Histopathology and immunohistochemistry of PDT-treated tumors confirmed the evidence of apoptosis compared with untreated tumors. **Conclusion:** These data demonstrate the detection of apoptosis using ^{99m}Tc-annexin V in tumor tissue in living animals after PDT treatment. This novel technique could be used as a noninvasive means to detect and serially image tissues undergoing apoptosis after cancer treatment protocols in humans. Other potential applications of this technique could be the diagnosis of several human disorders, such as myocardial ischemia or infarct, rejection of organ transplantation, and neonatal cerebral ischemia.

Key Words: apoptosis; annexin V; diagnostic imaging; photodynamic therapy; mouse model

J Nucl Med 2003; 44:650–656

Received May 24, 2002; revision accepted Oct. 24, 2002.

For correspondence or reprints contact: Urs O. Häfeli, PhD, The Cleveland Clinic Foundation, 9500 Euclid Ave., T28, Cleveland, OH 44195.

E-mail: hafeliu@ccf.org

Apoptosis or programmed cell death (*1*) is an essential life process for all cellular organisms. It is an active process of cellular self-destruction that plays an important role in a large number of disorders, including organ rejection after transplantation (*2*), myocardial ischemia or infarct (*3*), and neurodegenerative diseases (*4*). Apoptosis also plays a major role in cancer therapy. Apoptotic cell death occurs after the treatment of cancer by radiation, chemotherapy, and photodynamic therapy (PDT) (*5–7*). The extent and time at which apoptosis occurs may be important in elucidating potential clinical information in the management of cancer treatment protocols. For this reason, considerable efforts have been made in developing and validating methods to image apoptosis in vivo (*8–11*).

The 2 most promising techniques to detect apoptosis use either magnetic resonance spectroscopy or radionuclide imaging with radiolabeled annexin V. The first technique, detection of apoptosis in vivo using magnetic resonance spectroscopy is limited by relatively low sensitivity and poor spatial resolution (*12*). In the second technique, an early event in apoptosis, the redistribution of the membrane compound phosphatidylserine from the inner to the outer leaflet of the plasma membrane, is exploited (*13*). Annexin V, a human protein with a molecular weight of 36 kDa, has a high affinity for cells with exposed phosphatidylserine (*14*) and forms the basis of radiolabeled methods for detecting apoptosis in vivo (*11*). This technique is highly selective and good resolution for the detection of apoptosis is reached. Blankenberg et al. (*11*) have used 6-hydrazinonicotinamide (HYNIC)-annexin V and radiolabeled it with ^{99m}Tc in several time-consuming steps, which limits its use for routine clinical applications (*15*). In view of these difficulties, as a first aim, we developed a simpler method of labeling annexin V with ^{99m}Tc.

Our second aim was to explore the efficacy of the radiolabeled ^{99m}Tc-annexin V to image apoptosis during tumor

shrinkage after cancer treatment protocols. To accomplish this goal we used PDT to induce apoptosis during tumor shrinkage in a murine tumor model (*7,16,17*). PDT is a new modality for the treatment of cancers (*18*). It involves the administration of a photosensitizer followed by exposure of the tissue to visible laser light (630–800 nm). When the tissue homing the photosensitizer is illuminated with light of the appropriate wavelength, the molecule is excited and a series of molecular energy transfers are initiated. In the presence of oxygen in the tissue, this reaction leads to the generation of singlet oxygen, a highly reactive and cytotoxic species that results in cell death. The combination of selective photosensitizing drug uptake in malignant tissues and selective light delivery has the potential to effectively destroy tumors with limited damage to the surrounding normal tissue (*19*).

MATERIALS AND METHODS

Radiolabeling of Annexin V with ^{99m}Tc

To a 10-mL vial were added 4.0 mg of succinic dihydrazide (SDH), 4.0 mg of propylenediaminetetraacetic acid (PDTA), 20.0 mg of tricine, 2.0 mg of nicotinic acid, 50 μL (50 μg) of stannous chloride dihydrate in 0.1N HCl (2 mg/mL), and 300 μL of 0.5 mol/L phosphate buffer (pH 8.5; mixture A). The radioactive $^{99m}TcO_4^-$ (110 MBq) was then added in 30 μL of saline and kept at room temperature for 10 min. Forty micrograms (40 μL) of human annexin V (R & D System, Minneapolis, MN) were added and the mixture was heated at 90°C for 10 min with stirring at 1,400 rpm using an Eppendorf thermomixer (Brinkmann Instruments Co., Westbury, NY). The radiochemical purity of the complex was found to be >95%.

Kits of lyophilized marker were made by sterile filtrating mixture A into vial A and 40 μg of annexin V in 100 μL saline in vial B. Both were lyophilized in a Labconco freeze dryer 8 (Kansas City, MO) for 24 h and then stored in the freezer. Vial A was rehydrated by the addition of up to 740 MBq ^{99m}Tc in 400 μL of saline and incubated for 10 min at room temperature. Vial B with the annexin V was rehydrated for 10 min with 100 μL of distilled water. The radioactive mixture was added to the annexin V and heated at 90°C for 10 min.

Radiochemical Analysis by Instant Thin-Layer Chromatography

The radiochemical purity of ^{99m}Tc-annexin V was determined by ascending instant thin-layer chromatography (ITLC) with silica gel-coated fiberglass sheets (Gelman Sciences Inc., Ann Arbor, MI) using either physiologic saline (0.9% NaCl) or acidified 85% ethanol (pH 4) as the mobile phase. The radioactive contaminants were identified as reduced/hydrolyzed ^{99m}Tc and free $^{99m}TcO_4^-$. The radiolabeled annexin V was tested for its in vitro stability at 1, 3, 6, and 24 h after preparation at room temperature. In vitro plasma stability experiments were also performed by combining 100 μL ^{99m}Tc-annexin V and 100 μL of human plasma and incubating at 37°C. At each time point, 5-μL samples were removed, spotted on TLC strips, and analyzed as described. Radioactivity associated with the chromatographed ITLC strips was scanned using a radiation scanner. The radiochemical purity of the labeled annexin V was determined with Origin version 6.1 software (OriginLab Corp., Northampton, MA).

An additional stability test, the cysteine challenge, was performed by incubating 100 μL of 10 mmol/L cysteine with 100 μL of radiolabeled annexin V for 1 and 2 h and determining the free pertechnetate by ITLC using saline as solvent.

Size-Exclusion Chromatography

Radiolabeled annexin V was analyzed by gel-permeation chromatography using a Sephadex G-25 column (PD-10; Amersham Pharmacia Biotech AB, Uppsala, Sweden) equilibrated and eluted with 0.1 mol/L phosphate buffer (pH 7.4) at a flow rate of 1.0 mL/min. The eluent was collected in 1.0-mL fractions and the radioactivity associated with each fraction was measured in a Radcal dose calibrator (model 4050; Radcal Corp., Monrovia, CA). High-pressure liquid chromatography (HPLC) was also performed to analyze the radiolabeled product using a Gilson HPLC system with 307 pump and 119 UV/Vis detector with an analytic 20-cm Jordi Gel GPC mixed-bed column (Alltech Associates, Deerfield, IL). Elutions with 0.05 mol/L ammonium acetate buffer (pH 7) were performed at a flow rate of 1.0 mL/min with an injection volume of 20 μL of labeled annexin V. The run time was 20 min per sample, and the radiation was detected using a QC-2000 (Bioscan, Washington, DC).

Silicon Phthalocyanine Formulation and PDT of Tumors

Silicon phthalocyanine (Pc 4) was synthesized as described (*20*) and was procured from Dr. Malcolm Kenney (Department of Chemistry, Case Western Reserve University). A stock solution (1 mg/mL) was prepared as described (*18*) by dissolving solid Pc 4 in equal volumes of Cremophor EL (Sigma-Aldrich Co., St. Louis, MO) and absolute ethanol followed by the addition of 9 vol of 0.9% saline solution while vortexing at low speed. This solution was passed through a 0.22-μm membrane filter, and the concentration was determined by spectrophotometry, aliquoted, and stored at −26°C. For injection to tumor-bearing animals, the Pc 4 stock solution was mixed with an equal volume of 90% saline, 5% Cremophor EL, and 5% absolute ethanol as described (*16*).

All animal experiments were performed according to American Association of Laboratory Animal Care guidelines on an approved institutional animal protocol. C_3H mice were injected with 1.5×10^6 radiation-induced fibrosarcoma (RIF-1) tumor cells intradermally on the posterior dorsum (*21*). When tumors reached a volume of 40–60 mm^3 about 7–8 d after inoculation, 1.0 mg of Pc 4 per kg body weight was injected via tail vein as described (*7,16*). Forty-eight hours later the animals were restrained for light exposure. A 1-cm-diameter area encompassing the tumor was irradiated with laser light of 672 ± 2 nm at a fluence of 150 J/cm^2 (power density, 150 mW/cm^2) (Applied Optronics Corp., Newport, CT) via a 400-μm quartz fiber optic cable terminated in a microlens, thus distributing the light uniformly over the treatment field.

Tumor Imaging by Autoradiography

C_3H mice bearing RIF-1 tumors received 50 μL (5.55 MBq) of ^{99m}Tc-annexin V by tail vein injection at 2, 4, and 7 h after PDT treatment. Groups of 3 mice were imaged 1 h thereafter. For the autoradiography, PDT-treated and untreated control animals were simultaneously placed under anesthesia on a storage phosphor screen MP (Packard Instruments Co., Meriden, CT) and left there in the dark for 10 min. In addition, a small ^{137}Cs point source as a geometric marker was placed on the phosphor screen and an optical photograph of animals was taken. The autoradiographs were developed using a Cyclone Phosphor Imager (Packard Instruments Co.) and analyzed using Optiquant software (Packard

Instruments Co.). The position of the tumors with ^{99m}Tc-labeled areas was matched by overlaying autoradiographs and photographs using the software Image Pro Plus (Media Cybernetics, Silver Spring, MD).

Histopathology and Immunostaining

All tumors were fixed in 10% buffered formalin, paraffin embedded, cut in 5-μm sections, stained with hematoxylin and eosin, and evaluated by an experienced histopathologist. For immunostaining, the formalin-fixed paraffin-embedded tissue sections were deparaffinized, dehydrated, and incubated in 0.3% H_2O_2 in absolute methanol for 30 min to block endogenous peroxidase. Nonspecific staining was blocked using normal serum at a 1:50 dilution for 30 min, followed by incubation overnight at 4°C with specific primary antibodies against annexin V (goat polyclonal IgG; Santa Cruz Biotechnology, Santa Cruz, CA). Sections were then rinsed in phosphate-buffered saline and immunostained using a kit (Calbiochem, La Jolla, CA). A positive reaction was visualized as brown stain after incubating the slides with 3,3′-diaminobenzidine for 5 min. The sections were rinsed with distilled water, counterstained with Gill's hematoxylin for 1 min, and mounted with Universal Mount (Research Genetics, Huntsville, AL). Apoptotic cells (brown stained) were counted under the microscope using the Optimas 6 software program (Optimas Corp., Bothell, WA). The apoptotic index was calculated by dividing the number of apoptotic cells by the total number of cells counted per sample cross-section.

RESULTS

Annexin V was labeled with ^{99m}Tc using a simple and modified procedure in the presence of SDH, PDTA, tricine, and nicotinic acid at elevated temperatures. Heating at 90°C for 10 min was essential to achieving a radiochemical yield of >95%. The radiochemical purity of the labeled annexin V was evaluated by ITLC, which successfully resolved the labeled product from reduced/hydrolyzed ^{99m}Tc and free ^{99m}Tc pertechnetate (Fig. 1). The labeled preparations comprised >98% ^{99m}Tc-annexin V with the remainder being reduced/hydrolyzed ^{99m}Tc (~1%) and free ^{99m}Tc pertechnetate (~1%). The radiochemical stability of ^{99m}Tc-annexin V in saline at room temperature and in human plasma at 37°C was excellent (Table 1). Labeling tests with freshly made reagents or the lyophilized kit showed no difference in labeling efficiency and stability of the product.

TABLE 1
Radiochemical Stability of ^{99m}Tc-Annexin V in Saline and Plasma as Measured by TLC

Time point	Saline at room temperature (%)	Plasma at 37°C (%)
0 h	100	100
10 min	99.8 ± 1.3	99.8 ± 0.0
1 h	97.1 ± 2.1	96.9 ± 1.1
5 h	94.6 ± 3.5	95.2 ± 0.6
24 h	94.8 ± 6.4	94.0 ± 1.1

Data represent mean ± SD of 3 independent analyses.

Size-exclusion chromatography was used to characterize radiolabeled annexin V and free ^{99m}Tc, both on Sephadex and by HPLC. On a short PD-10 Sephadex column, we could clearly separate the radiolabeled ^{99m}Tc-annexin V with a peak at 7.5 mL from unlabeled annexin V at 9.5 mL, with free ^{99m}Tc-pertechnetate eluting at 13 mL (Fig. 2). This finding was confirmed by HPLC (Fig. 3). The ^{99m}Tc-annexin V complex eluted at a retention time of 10.1 min, whereas the free ^{99m}Tc eluted at 11.4 min. Figure 3 shows also a test mix of radiolabeled annexin V and pertechnetate because no free ^{99m}Tc was found in the ^{99m}Tc-annexin V. No attempts were made to characterize 2 small peaks before and after the ^{99m}Tc-annexin V peak. The peak before might be a dimer of annexin V.

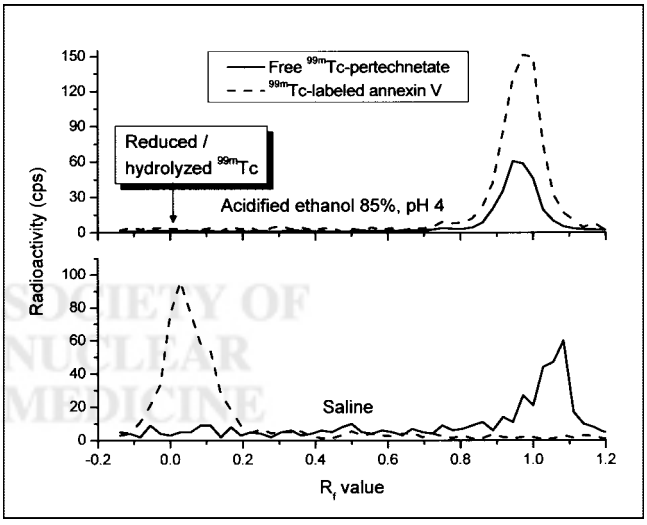

FIGURE 1. TLC of 1.48 MBq ^{99m}Tc-annexin V and ^{99m}Tc-pertechnetate with 2 different solvent systems.

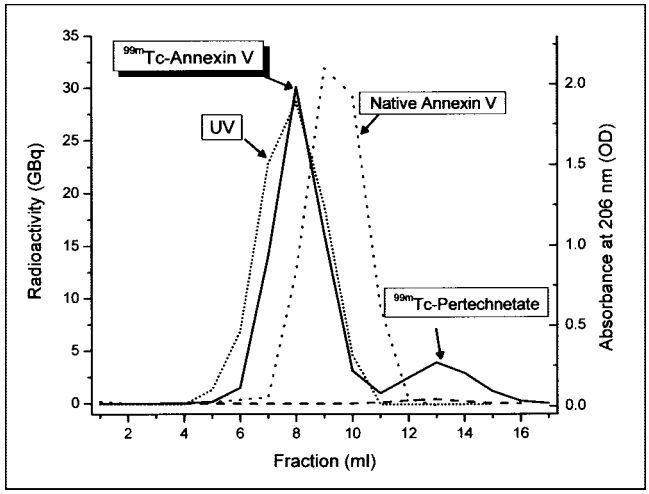

FIGURE 2. Radiochromatography of ^{99m}Tc-annexin V and $^{99m}TcO_4^-$ test mixture by size-exclusion chromatography. Unlabeled annexin V (40 μg) was also analyzed using UV spectroscopy at 206 nm.

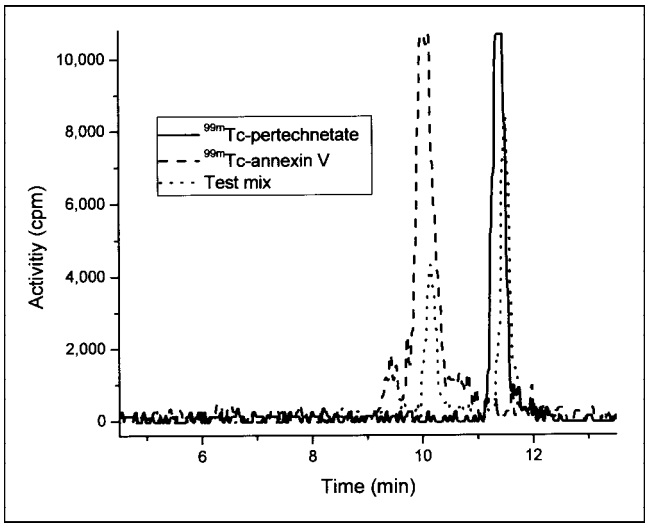

FIGURE 3. Elution profile of ^{99m}Tc-annexin V, ^{99m}Tc-pertechnetate, and test mixture at 1 h after labeling using HPLC.

The binding stability of ^{99m}Tc with annexin V was also confirmed with a cysteine challenge test at 37°C. Less than 1% of the total radioactivity was detected by ITLC after 1 or 2 h of incubation with 10 mmol/L cysteine as free pertechnetate, indicating the good stability of the labeled complex.

After successful labeling of annexin V with ^{99m}Tc and its characterization, we explored its imaging efficacy in an in vivo system. We took advantage of our earlier studies in which we have shown that PDT induces the rapid onset of apoptosis in vitro (*22*) and in vivo (*7*). After intravenous tail vein injection at 2, 4, and 7 h after PDT treatment, semiquantitative autoradiographs were obtained, showing a high concentration of radiolabeled annexin V in liver and kidneys of both control and PDT-treated mice (Figs. 4 and 5). An avid uptake of ^{99m}Tc-annexin V was observed in tumors treated with PDT after 2, 4, and 7 h, whereas no uptake was visualized in untreated control tumors (Figs. 4 and 5).

Some of the PDT-treated and nontreated tumor tissues were analyzed for apoptosis by histopathologic and immunohistochemical methods. Tumor sections treated with PDT showed extensive areas of myxoid degeneration, cellular involution, and marked vascular congestion, typically with foci of mixed, round cell, and neutrophil infiltrate (Fig. 6C). They were prominent as early as 2 h after PDT. These changes were highly pronounced and focally associated with hemorrhage (peliosis) 4 and 7 h after PDT (data not shown) and were not observed in the tumors of control animals (Fig. 6A). These observations are consistent with the findings reported by Blankenberg et al. (*11*).

Immunohistochemical studies showed that 66% ± 6% of the cells at the cytoplasmic border of apoptotic nuclei in the treated tumor stained positive for annexin V (Figs. 6D and 6E), correlating well with the localization of ^{99m}Tc-annexin V in the same tumors. Only 6.6% ± 1.4% staining was observed in tumor sections of control animals (Figs. 6B and 6E). Furthermore, we previously showed that RIF-1 tumor-bearing C_3H mice subjected to Pc 4-PDT had undergone increased DNA fragmentation at 2, 4, and 6 h after PDT, suggesting the increased apoptosis is a measure of Pc 4-PDT response. ^{99m}Tc-Annexin V uptake is a measure to detect the apoptosis induced by Pc 4-PDT.

DISCUSSION

Currently there is considerable interest in labeling small molecules with ^{99m}Tc for developing target-specific imaging agents (*23,24*). The agent HYNIC has been used extensively as a bifunctional coupling agent for the ^{99m}Tc labeling of small biomolecules for thrombus imaging (*25,26*), a chemotactic peptide for the diagnosis of infection and inflam-

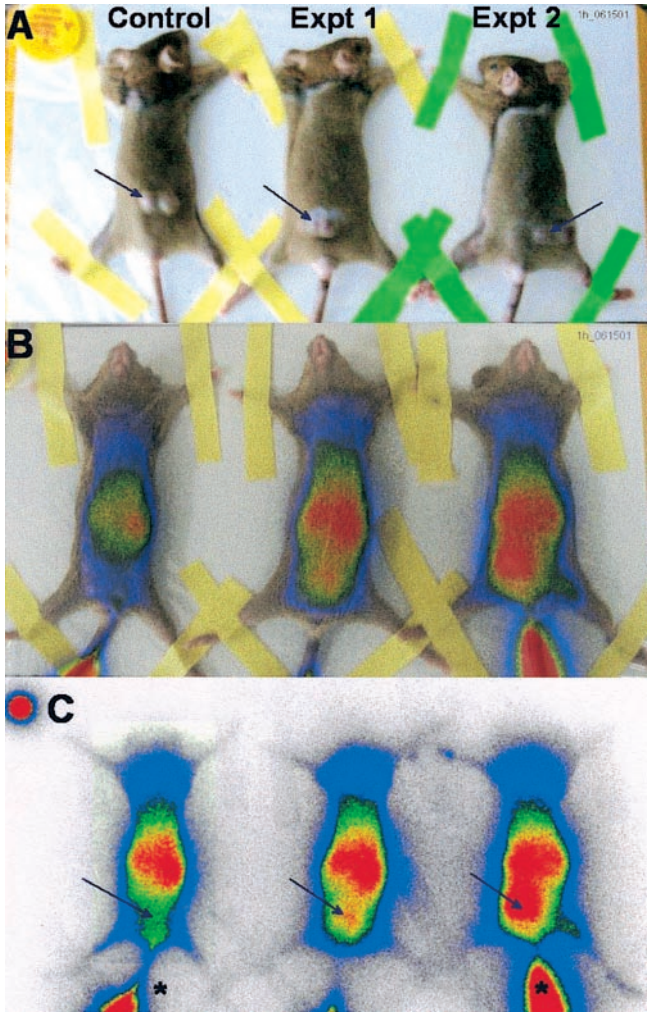

FIGURE 4. Autoradiography of PDT-treated and untreated C_3H mice bearing RIF-1 tumors after administration of ^{99m}Tc-annexin V. RIF-1 tumor-bearing mice were subjected to Pc 4-PDT, followed 2 h after PDT by tail vein injection of 5.55 MBq ^{99m}Tc-annexin V. One hour later autoradiographs were obtained using a phosphor screen. (A) Animals were positioned in prone position to show location of tumor. (B) Same animals turned in supine position while acquiring autoradiographs, overlaid with accumulated activity. (C) Autoradiographic images of same animals. Arrows indicate tumor location; stars indicate tail vein injection site.

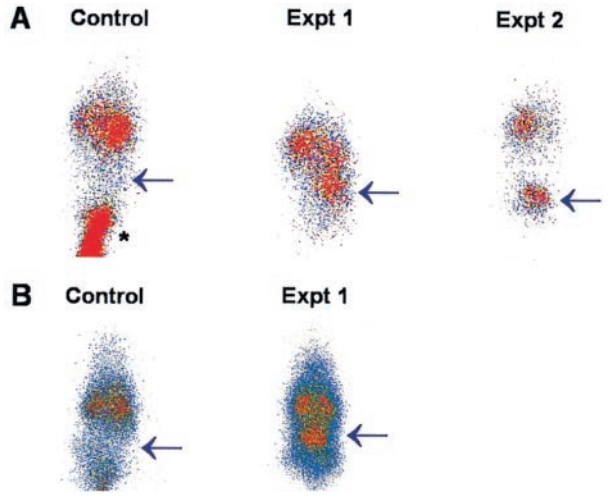

FIGURE 5. Images of untreated control and PDT-treated C_3H mice bearing RIF-1 tumors after administration of ^{99m}Tc-annexin V at 4 h (A) and 7 h (B) after PDT. Autoradiographs were taken 1 h after injection with animals placed in supine position on phosphor screen. Arrows indicate tumor location; star indicates tail vein injection site.

mation (*27*,*28*), and LTB_4 receptor antagonists for imaging infection, inflammation (*29*), and apoptosis (*11*). HYNIC has been found to be very useful for achieving stable technetium complexes in connection with tricine and phosphine as coligands, which are necessary to complete the coordination sphere of the technetium core along with the HYNIC-biomolecules (*25*). Unfortunately, the conjugation procedure of HYNIC with specific biomolecules is tedious and cumbersome, and the efficiency is often not optimal.

In this study we have successfully radiolabeled annexin V with ^{99m}Tc and demonstrated its usefulness in detecting apoptosis induced by Pc 4-PDT in RIF-1 tumors. We used SDH in the presence of tricine, nicotinic acid, PDTA, and stannous chloride to label annexin V with ^{99m}Tc. SDH was chosen as the donor of the nitride nitrogen atom N_3^-. PDTA was added to prevent the precipitation of Sn^{2+} in the form of insoluble tin salts. The method is based on the reaction of ^{99m}Tc with SDH or annexin V in the presence of stannous chloride as a reducing agent to form the ^{99m}Tc-annexin V complex. Tricine and nicotinic acid act as coligand and ternary ligand, respectively, and lead to good radiochemical yield and stability of the product. The structure of the final product very likely involves $[Tc{\equiv}N]^{2+}$ that binds to 1 or more sites that involve histidine and cysteine molecules of annexin V (*23*,*30*). However, the binding of tricine and nicotinic acid to the other side of the technetium core to form an efficient chelating moiety cannot be ruled out. Because there appears to be a Ca^{2+} binding site in annexin molecules, it has been found that divalent metal ions bind to annexin V. It is possible that $[Tc{\equiv}N]^{2+}$ binds to the site where Ca^{2+} normally binds and the annexin-mediated aggregation is more selective to metal ions than the binding to membranes (*31*).

Because a radiochemical yield of >95% was achieved, no additional purification or extraction steps were necessary. Furthermore, this simple procedure can be called a 1-pot method and is thus easier to perform than other currently available methods (*32*,*33*). The development of a freeze-dried kit formulation has been successful and the kit is now in routine laboratory use.

The radiochemical stability of the labeled complex in plasma was found to be 94% 24 h after preparation, which would be adequate for clinical applications. Interestingly, stability measurements in saline yielded similar results (Table 1). Combined with the results from the cysteine challenge test, it seems that radiolabeled ^{99m}Tc-annexin V is able to withstand blood components, such as cysteine or glutathione, that typically attack chelated radioisotopes.

The labeled annexin V was characterized both by size-exclusion chromatography and by ITLC. The order of elu-

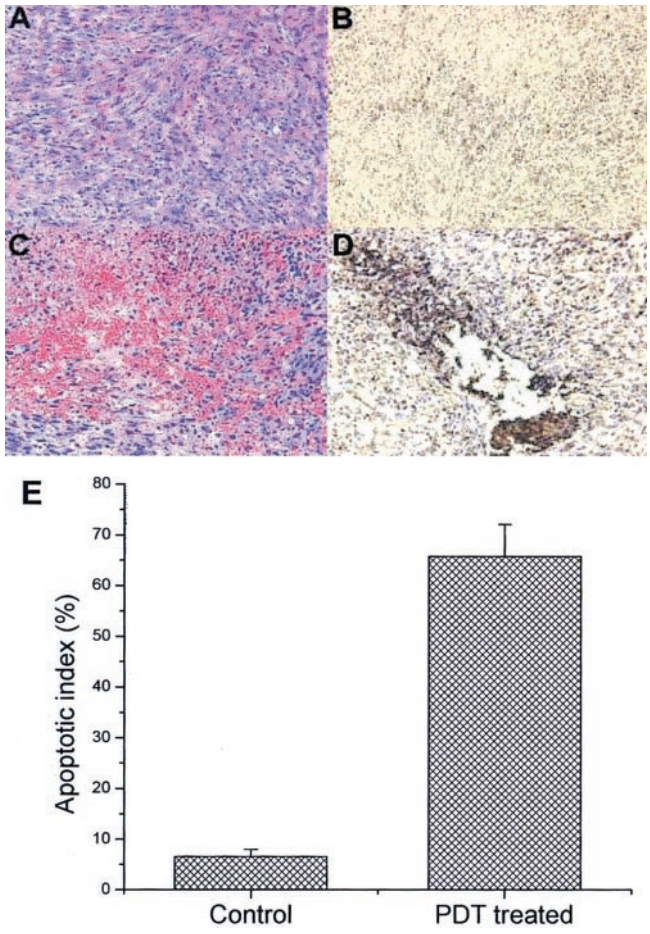

FIGURE 6. Photomicrographs of tissue sections of PDT-treated and untreated RIF-1 tumors. (A) Hematoxylin and eosin–stained control tumor section. (B) Immunohistochemical expression of annexin V in control animals. Cells expressing apoptotic bodies are stained brown. (C) Hematoxylin and eosin–stained tumor section 2 h after PDT. (D) Immunohistochemical expression of annexin V in tumor section 2 h after PDT. (E) Apoptotic index, expressed as percentage of all cells that contained immunohistologically brown-stained apoptotic cells in untreated control and PDT-treated tumor sections.

tion from the PD-10 column—namely, first the radiolabeled annexin V, then the unlabeled annexin V, and then free ^{99m}Tc—agreed well with the molecular weight of the compounds (Fig. 2). Radiolabeled annexin V, which contains additional molecules such as SDH, tricine, nicotinic acid, and PDTA, is thus larger and can be separated from unlabeled annexin V. The exact structure of the compound, however, is not known yet.

The purity of radiolabeled annexin V was further analyzed by HPLC (Fig. 3). The radioactive peak obtained at a retention time of 10.1 min corresponded with annexin V. No peak appeared at a retention time of 11.4 min, indicating that no free pertechnetate was present in the labeled complex. These results were thus consistent with the ITLC and PD-10 measurements and confirmed the radiochemical purity of the labeled annexin V.

The efficiency of ^{99m}Tc-annexin V as an apoptosis imaging agent was investigated in a murine RIF-1 tumor model system that had undergone rapid onset of apoptosis after PDT treatment. The radioactivity was mainly found in the abdominal region, predominantly in the intestines, liver, and kidneys, suggesting that ^{99m}Tc-annexin V is excreted through the kidneys and reticuloendothelial system. The increased intestinal uptake seen here will very likely make our method not suitable for evaluation of apoptosis of abdominal tumors. There was insignificant change in renal and liver uptake of ^{99m}Tc-annexin V in PDT treated mice compared with control animals. The mechanism(s) of increased uptake in kidney and liver is not clear but may relate to the intrinsic lipid profile of these organs or the nonspecific scavenging of proteins such as annexin V. It has been reported that renal distribution of radiolabeled annexin V is cortical (*11*). This could be related to the high phospholipid composition of the renal cortex, which is rich in phosphatidylserine compared with the papillary region (*34*). The other possible explanation could be the nonspecific uptake of low-molecular-weight proteins such as annexin V by the proximal renal tubule cells noted in studies of peptides and antibody fragments (*35*).

An excellent uptake of ^{99m}Tc-annexin V was observed in tumors treated with PDT, whereas no radioactivity was visualized in untreated control tumors (Figs. 4 and 5). PDT treatment of these tumors has been shown to induce apoptosis rapidly even 1 h after PDT (*7*). Therefore, we concluded that the higher tumor uptake in PDT-treated animals was due to apoptosis, as was further substantiated by autoradiographic, histopathologic, and immunohistochemical studies. Autoradiography with ^{99m}Tc-annexin V demonstrated clear and specific localization of regions of apoptotic cell death in a simple way and without the use of a gamma camera. This novel technique can directly assess an early event of programmed cell death that could not be visualized and quantified by other techniques. It should prove more useful than lipid proton nuclear magnetic resonance spectroscopy (*12*), which, to date, is the only method available to detect apoptosis noninvasively in vivo, but has an inherent problem of low sensitivity.

The induction of apoptosis after PDT has been shown to be very rapid (*7*) and, therefore, 2 h suffice to clearly visualize cell death. Later time points were histologically more pronounced but did not add much to the imaging information obtained at 2 h (Fig. 4). Binding of the radiolabeled compound to cells undergoing apoptosis is also very fast, and 1 h between injection of the compound and radionuclide imaging was found to be satisfactory. However, early time-course phosphor imaging studies need to be performed to ascertain the optimal time for achieving high tumor-to-nontumor ratios. Clinical imaging studies could thus be scheduled and performed conveniently 1–2 h after injection on the same day of (cancer) treatment.

Sections from tumors treated with PDT showed extensive cellular morphologic changes such as myxoid degeneration, cellular involution, and marked vascular congestion (Fig. 6C). These changes were highly associated with hemorrhage (peliosis) at all time points and agreed well with findings of Blankenberg et al. (*11*). Immunohistochemical studies showed that >65% of the nuclei stained positive for annexin V antibodies (Fig. 6D) in the treated tumor at all time points, in contrast to 6.6% of the untreated control tumors (Fig. 6B). The increase in phosphatidylserine expression associated with rapid cell death can thus be successfully imaged with ^{99m}Tc-annexin V prepared with our novel labeling method.

In summary, we conclude that noninvasive detection and serial imaging of organs or tissues undergoing apoptosis and necrosis in vivo are possible. After standardization of the procedure for an indication, this method could prove useful, for example, in reducing multiple biopsies after cardiac transplantation. The ability of ^{99m}Tc-annexin V to clinically diagnose apoptosis in cardiac allograft recipients has been recently demonstrated by Narula et al. (*36*) in 5 patients showing histologic evidence of transplant rejection. The ability to image apoptosis in vivo may lead to more expeditious and precise assessment of therapeutic interventions. Therefore, this agent could be of use in evaluating the efficacy of cancer therapies and disease progression or regression. Especially useful would be its use for diagnostic imaging of cancer patients, who are starting a new treatment modality after failing a previous therapy. Serial treatment failures with affiliated waste of money and time, and endured side effects of these highly toxic treatments, could thus be avoided.

CONCLUSION

There are 2 unique aspects of this study. First, a novel method for the development of ^{99m}Tc labeling of annexin V has been developed. The procedure described is a 1-pot labeling procedure, which made it possible to develop a freeze-dried kit formulation suitable for use in a hospital radiopharmacy. Second, we have shown the usefulness of

^{99m}Tc-labeled annexin V for the noninvasive imaging of apoptosis during tumor regression induced by PDT. This method may provide an excellent approach to monitor tumor response and efficacy of cancer treatment protocols and help in diagnosing several human disorders, such as myocardial ischemia or infarct, rejection of organ transplantation, and neonatal cerebral ischemia.

ACKNOWLEDGMENTS

We thank Dr. Roger Macklis (Radiation Oncology Department, The Cleveland Clinic Foundation), who provided the laboratory space for carrying out the study. We also thank Dr. Gopal Saha and Kanak Amin (Radiopharmacy, The Cleveland Clinic Foundation) for supplying the ^{99m}Tc. This study was supported by U.S. Public Health Service grants PO1 CA 48735, RO1 CA 51802, and RO1 CA 78803.

REFERENCES

1. Kerr JFR, Harmon BV. Definition and incidence of apoptosis: a historical perspective. In: Tomei LD, Cope FO, eds. *Apoptosis: The Molecular Basis of Cell Death.* Cold Spring Harbor, NY: Cold Spring Harbor Laboratory Press; 1991:5–29.
2. Kabelitz D. Apoptosis, graft rejection, and transplantation tolerance. *Transplantation.* 1998;65:869–875.
3. Mattson MP, Culmsee C, Yu ZF. Apoptotic and antiapoptotic mechanisms in stroke. *Cell Tissue Res.* 2000;301:173–187.
4. Thompson CB. Apoptosis in the pathogenesis and treatment of disease. *Science.* 1995;267:1456–1462.
5. Meyn RE, Stephens LC, Ang KK, et al. Heterogeneity in the development of apoptosis in irradiated murine tumours of different histologies. *Int J Radat Biol.* 1993;64:583–591.
6. Meyn RE, Stephens LC, Hunter NR, Milas L. Apoptosis in murine tumors treated with chemotherapy agents. *Anticancer Drugs.* 1995;6:443–450.
7. Zaidi SIA, Oleinick NL, Tarif Zaim M, Mukhtar H. Apoptosis during photodynamic therapy-induced ablation of RIF-1 tumors in C3H mice: electron microscopic, histopathologic and biochemical evidence. *Photochem Photobiol.* 1993; 58:771–776.
8. Czarnota GJ, Kolios MC, Abraham J, et al. Ultrasound imaging of apoptosis: high-resolution non-invasive monitoring of programmed cell death in vitro, in situ and in vivo. *Br J Cancer.* 1999;81:520–527.
9. Zucker RM, Hunter ES 3rd, Rogers JM. Apoptosis and morphology in mouse embryos by confocal laser scanning microscopy. *Methods.* 1999;18:473–480.
10. Hakumaki JM, Poptani H, Sandmair AM, Yla-Herttuala S, Kauppinen RA. ^{1}H MRS detects polyunsaturated fatty acid accumulation during gene therapy of glioma: implications for the in vivo detection of apoptosis. *Nat Med.* 1999;5: 1323–1327.
11. Blankenberg FG, Katsikis PD, Tait JF, et al. In vivo detection and imaging of phosphatidylserine expression during programmed cell death. *Proc Natl Acad Sci USA.* 1998;95:6349–6354.
12. Blankenberg FG, Katsikis PD, Storrs RW, et al. Quantitative analysis of apoptotic cell death using proton nuclear magnetic resonance spectroscopy. *Blood.* 1997; 89:3778–3786.
13. Emoto K, Toyama-Sorimachi N, Karasuyama H, Inoue K, Umeda M. Exposure of phosphatidylethanolamine on the surface of apoptotic cells. *Exp Cell Res.* 1997;232:430–434.
14. Wood BL, Gibson DF, Tait JF. Increased erythrocyte phosphatidylserine exposure in sickle cell disease: flow-cytometric measurement and clinical associations. *Blood.* 1996;88:1873–1880.
15. Kemerink GJ, Boersma HH, Thimister PW, et al. Biodistribution and dosimetry of ^{99m}Tc-BTAP-annexin V in humans. *Eur J Nucl Med.* 2001;28:1373–1378.
16. Colussi VC, Feyes DK, Mulvihill JW, et al. Phthalocyanine 4 (Pc 4) photodynamic therapy of human OVCAR-3 tumor xenografts. *Photochem Photobiol.* 1999;69:236–241.
17. Whitacre CM, Feyes DK, Satoh T, et al. Photodynamic therapy with the phthalocyanine photosensitizer Pc 4 of SW480 human colon cancer xenografts in athymic mice. *Clin Cancer Res.* 2000;6:2021–2027.
18. Kalka K, Merk H, Mukhtar H. Photodynamic therapy in dermatology. *J Am Acad Dermatol.* 2000;42:389–413.
19. Pass HI. Photodynamic therapy in oncology: mechanisms and clinical use. *J Natl Cancer Inst.* 1993;85:443–456.
20. Agarwal ML, Larkin HE, Zaidi SI, Mukhtar H, Oleinick NL. Phospholipase activation triggers apoptosis in photosensitized mouse lymphoma cells. *Cancer Res.* 1993;53:5897–5902.
21. Twentyman PR, Brown JM, Gray JW, Franko AJ, Scoles MA, Kallman RF. A new mouse tumor model system (RIF-1) for comparison of end-point studies. *J Natl Cancer Inst.* 1980;64:595–604.
22. Agarwal ML, Clay ME, Harvey EJ, Evans HH, Antunez AR, Oleinick NL. Photodynamic therapy induces rapid cell death by apoptosis in L5178Y mouse lymphoma cells. *Cancer Res.* 1991;51:5993–5996.
23. Liu S, Edwards DS. ^{99m}Tc-Labeled small peptides as diagnostic radiopharmaceuticals. *Chem Rev.* 1999;99:2235–2268.
24. Boerman OC, Oyen WJ, Corstens FH. Radiolabeled receptor-binding peptides: a new class of radiopharmaceuticals. *Semin Nucl Med.* 2000;30:195–208.
25. Edwards DS, Liu S, Barrett JA, et al. New and versatile ternary ligand system for technetium radiopharmaceuticals: water soluble phosphines and tricine as coligands in labeling a hydrazinonicotinamide-modified cyclic glycoprotein IIb/IIIa receptor antagonist with ^{99m}Tc. *Bioconjug Chem.* 1997;8:146–154.
26. Barrett JA, Damphousse DJ, Heminway SJ, et al. Biological evaluation of ^{99m}Tc-labeled cyclic glycoprotein IIb/IIIa receptor antagonists in the canine arteriovenous shunt and deep vein thrombosis models: effects of chelators on biological properties of ^{99m}Tc-chelator-peptide conjugates. *Bioconjug Chem.* 1996;7:203–208.
27. Edwards DS, Liu S, Ziegler MC, et al. A stabilized technetium-99m complex of a hydrazino nicotinamide derivatized chemotactic peptide for infection imaging. *Bioconjug Chem.* 1999;10:884–891.
28. Blankenberg FG, Tait JF, Blankenberg TA, Post AM, Strauss HW. Imaging macrophages and the apoptosis of granulocytes in a rodent model of subacute and chronic abscesses with radiolabled monocyte chetmotactic peptide-1 and annexin V. *Eur J Nucl Med.* 2001;28:1384–1393.
29. Liu S, Harris AR, Williams NE, Edwards DS. ^{99m}Tc-labeling of a hydrazinonicotinamide-conjugated LTB4 receptor antagonist useful for imaging infection and inflammation. *Bioconjug Chem.* 2002;13:881–886.
30. Tait JF, Smith C, Gibson DF. Development of annexin V mutants suitable for labeling with Tc(I)-carbonyl complex. *Bioconjug Chem.* 2002;13:1119–1123.
31. Mel'gunov VI, Akimova EI, Krasavchenko KS. Effect of divalent metal ions on annexin-mediated aggregation of asolectin liposomes. *Acta Biochim Pol.* 2000; 47:675–683.
32. Larsen SK, Solomon HF, Caldwell G, Abrams MJ. ^{99m}Tc-Tricine: a useful precursor complex for the radiolabeling of hydrazino nicotinate protein conjugates. *Bioconjug Chem.* 1995;6:635–638.
33. Abrams MJ, Juweid M, tenKate CI, et al. Technetium-99m-human polyclonal IgG radiolabeled via the hydrazino nicotinamide derivative for imaging focal sites of infection in rats. *J Nucl Med.* 1990;31:2022–2028.
34. Sterin-Speziale N, Kahane VL, Setton CP, Fernandez MC, Speziale EH. Compartmental study of rat renal phospholipid metabolism. *Lipids.* 1992;27:10–14.
35. Lang L, Jagoda E, Wu C, et al. Factors influencing the in vivo pharmacokinetics of peptides and antibody fragments: the pharmacokinetics of two PET-labeled low molecular weight proteins. *J Nucl Med.* 1997;41:53–61.
36. Narula J, Acio ER, Narula N, et al. Annexin-V imaging for noninvasive detection of cardiac allograft rejection. *Nat Med.* 2001;7:1347–1352.